Significant and variable linear polarization during a bright prompt optical flash

E. Troja[1,2], V. M. Lipunov[3,4], C. G. Mundell[5], N. R. Butler[6], A. M. Watson[7], S. Kobayashi[8], S. B. Cenko[2,1], F. E. Marshall[2], R. Ricci[9], A. Fruchter[10], M. H. Wieringa[11], E. S. Gorbovskoy[3,4], V. Kornilov[3,4], A. Kutyrev[1,2], W. H. Lee[7], V. Toy[1], N. V. Tyurina[3,4], N. M. Budnev[12], D. A. H. Buckley[13], J. González[7], O. Gress[12], A. Horesh[14], M. I. Panasyuk[15], J. X. Prochaska[16], E. Ramirez-Ruiz[16], R. Rebolo Lopez[17], M. G. Richer[18], C. Román-Zúñiga[18], M. Serra-Ricart[17], V. Yurkov[19], and N. Gehrels[2]

[1]Department of Astronomy, University of Maryland, College Park, MD 20742-4111, USA

[2]NASA Goddard Space Flight Center, 8800 Greenbelt Rd, Greenbelt, MD 20771, USA

[3]M.V. Lomonosov Moscow State University, Physics Department, Leninskie Gory, GSP-1, Moscow 119991, Russia

[4]M.V. Lomonosov Moscow State University, Sternberg Astronomical Institute, Universitetsky pr., 13, Moscow 119234, Russia

[5]Department of Physics, University of Bath, Claverton Down, Bath, BA2 7AY, UK

[6]School of Earth & Space Exploration, Arizona State University, AZ 85287, USA

[7]Instituto de Astronomía, Universidad Nacional Autónoma de México, Apartado Postal 70-264, 04510 Cd. de México, México

[8]Astrophysics Research Institute, Liverpool John Moores University, IC2 Building, Liverpool Science Park, 146 Brownlow Hill, Liverpool L3 5RF, United Kingdom

[9]INAF-Istituto di Radioastronomia, Via Gobetti 101, I-40129 Bologna, ITALY

[10]Space Telescope Science Institute, 3700 San Martin Drive, Baltimore, MD 21218, USA

[11]CSIRO Astronomy and Space Science, PO Box 76, Epping NSW 1710, Australia

[12]Irkutsk State University, Applied Physics Institute, 20, Gagarin Blvd, 664003 Irkutsk, Russia

[13]South African Astronomical Observatory, PO Box 9, 7935 Observatory, Cape Town, South Africa

[14]Racah Institute of Physics, Hebrew University, Jerusalem, 91904, Israel

[15]Skobeltsyn Institute of Nuclear Physics of Lomonosov, Moscow State University, Vorob'evy Gory, 119991 Moscow, Russia

[16]University of California Observatories, 1156 High St., Santa Cruz, CA 95064 USA

[17]Instituto de Astrofísica de Canarias Via Lactea, s/n E38205, La Laguna (Tenerife), Spain

[18]Instituto de Astronomía, Universidad Nacional Autónoma de México, Apartado Postal 106, 22800 Ensenada, Baja California, México

[19]Blagoveschensk State Pedagogical University, Lenin str., 104, Amur Region, Blagoveschensk 675000, Russia

Measurement of polarized light provides a direct probe of magnetic fields in collimated outflows (jets) of relativistic plasma from accreting stellar-mass black holes at cosmological distances. These outflows power brief and intense flashes of prompt gamma-rays known as Gamma Ray Bursts (GRBs), followed by longer-lived afterglow radiation detected across the electromagnetic spectrum. Rapid-response polarimetric observations of newly discovered GRBs have probed the initial afterglow phase[1-3]. Linear polarization degrees as high as Π≥30% are detected minutes after the end of the prompt GRB emission, consistent with a stable, globally ordered magnetic field permeating the jet at large distances from the central source[3]. In contrast, optical[4-6] and gamma-ray[7-9] observations during the prompt

phase led to discordant and often controversial[10-12] results, and no definitive conclusions on the origin of the prompt radiation or the configuration of the magnetic field could be derived. Here we report the detection of linear polarization of a prompt optical flash that accompanied the extremely energetic and long-lived prompt gamma-ray emission from GRB 160625B. Our measurements probe the structure of the magnetic field at an early stage of the GRB jet, closer to the central source, and show that the prompt GRB phase is produced via fast cooling synchrotron radiation in a large-scale magnetic field advected from the central black hole and distorted from dissipation processes within the jet.

On 25 June 2016 at 22:40:16.28 Universal Time (UT), the Gamma-Ray Burst Monitor (GBM) aboard NASA's *Fermi* Gamma-ray Space Telescope discovered GRB 160625B as a short- lived (≈1 s) pulse of γ-ray radiation (G1 in Fig. 1). An automatic localization was rapidly distributed by the spacecraft allowing wide-field optical facilities to start follow-up observations. Three minutes after the first alert, at 22:43:24.82 UT (hereafter T_0), the Large Area Telescope (LAT) aboard *Fermi* triggered on another bright and longer lasting (≈30 s) pulse (G2 in Fig. 1) visible up to GeV energies[13]. A rapid increase in brightness was simultaneously observed at optical wavelengths (Fig. 1). The optical light rose by a factor of 100 in a few seconds reaching its peak at T_0+5.9 s with an observed visual magnitude of 7.9. After a second fainter peak at T_0+15.9 s, the optical light is seen to steadily decline. During this phase the MASTER[14]-IAC telescope simultaneously observed the optical counterpart in two orthogonal polaroids starting at T_0+95 s and ending at T_0+360 s. A detection of a polarized signal with this instrumental configuration provides a lower bound to the true degree of linear polarization, $\Pi_{L,min} = (I_2 - I_1) / (I_1 + I_2)$ where I_1 and I_2 refer to the source intensity in each filter. Significant levels of linear polarization of up to $\Pi_{L,min}$=8.0±0.5% were detected compared with values <2% for other nearby objects with

similar brightness (Fig. 2). Over this time interval a weak tail of gamma-ray emission is visible until the onset of a third longer lived episode of prompt gamma-ray radiation (G3), starting at T_0+337 s and ending at T_0+630 s.

In the standard GRB model[15,16], after the jet is launched dissipation processes within the ultra-relativistic flow produce a prompt flash of radiation, mostly visible in gamma-rays. Later, the jet outermost layers interact with the surrounding medium and two shocks develop, one propagating outward into the external medium (forward shock) and the other one traveling backward into the jet (reverse shock). These shocks heat up the ambient electrons, which emit, via synchrotron emission, a broadband afterglow radiation. At very early time ($\lesssim T_0$+10 s) the observed optical flux from GRB 160625B is orders of magnitude brighter than the extrapolated prompt emission component (Fig. 3), suggesting that optical and gamma-ray emission originate from different physical locations in the flow. A plausible interpretation is that the early ($\lesssim T_0$+10 s) optical emission arises from a strong reverse shock, although internal dissipation processes are also possible (see Methods). A general prediction of the reverse shock model[17] is that, after reaching its peak, the optical flash should decay as a smooth power-law with slope of -2. However, in our case, the optical light curve is more complex: its temporal decay is described by a series of power-law segments with slopes between -0.3 and -1.8. The shallower decay could be in part explained by the ejection of a range of Lorentz factors, as the blastwave is refreshed by the arrival of the slower moving ejecta[18]. However, this would require ad-hoc choices of the Lorentz factor distribution in order to explain each different power-law segment and does not account for the observed temporal evolution of the polarization. Our observations are more naturally explained by including a second component of emission in the optical range, which dominates for $T>T_0$+300 s. Our broadband spectral analysis (see Methods) rules out a significant

92 contribution from the forward shock, whose emission is negligible at this time (f_{FS}<1 mJy).
93 Instead, the prompt optical component makes a substantial contribution (>40%) to the observed
94 optical light (Fig. 3).
95 The only other case of a time-resolved polarimetric study[3] showed that the properties of the
96 reverse shock remain roughly constant in time. Our measurements hint at a different temporal
97 trend. The fractional polarization appears stable over the first three exposures, and changes with
98 high significance (≈99.9996%) in the last temporal bin (Fig. 2). Based on our broadband dataset
99 we can confidently rule out geometric effects as the cause of the observed change. If the
100 observer's line of sight intercepts the jet edges, it would cause a steeper decay of the optical flux
101 and is also not consistent with the detection of an achromatic jet-break at much later times
102 (Extended Data Figure 1). The temporal correlation between the gamma-ray flux and the
103 fractional polarization (Fig. 2) and the significant contribution of the prompt component to the
104 optical emission (Fig. 3) suggest that the gamma-ray and optical photons are co-located and that
105 the observed variation in $\Pi_{L,min}$ is connected to the renewed jet activity. Thus our last observation
106 detected the linear optical polarization of the prompt emission, directly probing the jet properties
107 at the smaller radius from where prompt optical and gamma-ray emissions originate.
108 Three main emission mechanisms are commonly invoked to explain the prompt GRB phase, and
109 all three of them can in principle lead to a significant level of polarization. Inverse Compton (IC)
110 scattering and photospheric emission could lead to non-zero polarization only if the spherical
111 symmetry of the emitting patch is broken by the jet edges. However, as explained above, an off-
112 axis model is not consistent with our dataset. Furthermore, an IC origin of the observed prompt
113 phase would imply a prominent high-energy (>1 GeV) component, in contrast with the
114 observations[19]. The most plausible source of the observed photons is synchrotron radiation from

a population of fast cooling electrons moving in strong magnetic fields. This can account for the low-energy spectral slope $\alpha \sim -1.5$ (see Methods) and the high degree of polarization. An analogous conclusion, based on different observational evidence, was reached by an independent work on this burst[19].

If the magnetic field is produced by local instabilities in the shock front, the polarized radiation would come from a number of independent patches with different field orientations. This model does not reproduce well our data. It predicts erratic fluctuations of the polarization angle and a maximum level of polarization[20,21] $\Pi_{MAX} \approx \Pi_{syn}/\sqrt{N} \approx 2\text{-}3\%$ where $\Pi_{syn} \approx 70\%$ is the intrinsic polarization of the synchrotron radiation[22], and $N \approx 1{,}000$ is the number of magnetic patches[23]. Our observations are instead easily accommodated by a large-scale magnetic field advected from the central source. Recent claims of a variable polarization angle during the prompt γ-ray emission hinted, although not unambiguously, at a similar configuration[9].

This model[21,24] can explain the stable polarization measurements, the high degree of polarization, and its rapid change simultaneous with the onset of the new prompt episode. In this model the magnetic field is predominantly toroidal, and the polarization angle is constant. If relativistic aberration is taken into account[24], the polarization degree can be as high as $\approx 50\%$. In this case the probability of measuring a polarization as low as $\Pi_{L,min} \sim 8\%$ is approximately 10% (see Methods). It appears more likely that the actual polarization degree is lower than the maximum possible value and closer to our measurement, suggesting that the large-scale magnetic field might be significantly distorted by internal collisions[25,26] or kink instabilities[27] at smaller radii before the reconnection process produces bright gamma-rays.

Our results suggest that GRB outflows might be launched as Poynting flux dominated jets whose magnetic energy is rapidly dissipated close to the source, after which they propagate as hot

baryonic jets with a relic magnetic field. A large-scale magnetic field is therefore a generic property of GRB jets and the production of a bright optical flash depends on how jet instabilities develop near the source and their efficiency in magnetic suppression. The dissipation of the primordial magnetic field at the internal radius, as observed for GRB 160625B, is critical for the efficient acceleration of particles to the highest ($>10^{20}$ eV) energies[25,28]. However, the ordered superluminal component at the origin of the observed polarization and the relatively high magnetization ($\sigma \sim 0.1$; see Methods) of the ejecta might hinder particle acceleration through shocks[28], thus suggesting that either GRBs are not sources of ultra high-energy cosmic-rays as bright as previously thought or that other acceleration mechanisms[29] need to be considered.

1. Mundell, C. G., Steele, I. A., Smith, R. J., et al. Early Optical Polarization of a Gamma- Ray Burst Afterglow. *Science* **315**, 1822-1824 (2007)
2. Steele, I. A., Mundell, C. G., Smith, R. J., Kobayashi, S., & Guidorzi, C. Ten per cent polarized optical emission from GRB090102. *Nature* **462**, 767-769 (2009)
3. Mundell, C. G., Kopač, D., Arnold, D. M., et al. Highly polarized light from stable ordered magnetic fields in GRB 120308A. *Nature* **504**, 119-121 (2013)
4. Kopač, D., Mundell, C. G., Japelj, J., et al. Limits on Optical Polarization during the Prompt Phase of GRB 140430A. *Astrophys. J.* **813**, 1 (2015)
5. Pruzhinskaya, M. V., Krushinsky, V. V., Lipunova, G. V., et al. Optical polarization observations with the MASTER robotic net. *New Astronomy* **29**, 65-74 (2014)
6. Gorbovskoy, E. S., Lipunov, V. M., Buckley, D. A. H., et al. Early polarization observations of the optical emission of gamma-ray bursts: GRB 150301B and GRB 150413A. *Mon. Not. R. Astron. Soc.* **455**, 3312-3318 (2016)

7. Coburn, W., & Boggs, S. E. Polarization of the prompt γ-ray emission from the γ-ray burst of 6 December 2002. *Nature* **423**, 415-417 (2003)
8. Götz, D., Laurent, P., Lebrun, F., Daigne, F., & Bošnjak, Ž. Variable Polarization Measured in the Prompt Emission of GRB 041219A Using IBIS on Board INTEGRAL. *Astrophys. J.* **695**, L208-L212 (2009)
9. Yonetoku, D., Murakami, T., Gunji, S., et al. Magnetic Structures in Gamma-Ray Burst Jets Probed by Gamma-Ray Polarization. *Astrophys. J.* **758**, L1 (2012)
10. Rutledge, R. E., & Fox, D. B. Re-analysis of polarization in the γ-ray flux of GRB 021206. *Mon. Not. R. Astron. Soc.* **350**, 1288-1300 (2004)
11. McGlynn, S., Clark, D. J., Dean, A. J., et al. Polarization studies of the prompt gamma-ray emission from GRB 041219a using the spectrometer aboard INTEGRAL. *Astron. Astrophys.* **466**, 895-904 (2007)
12. Kalemci, E., Boggs, S. E., Kouveliotou, C., Finger, M., & Baring, M. G. Search for Polarization from the Prompt Gamma-Ray Emission of GRB 041219a with SPI on INTEGRAL. *Astrophys. J. Supp.* **169**, 75-82 (2007)
13. Dirirsa, F., GRB 160625B: Fermi-LAT detection of a bright burst. *GCN Circ.* 19580 (2016)
14. Lipunov, V., Kornilov, V., Gorbovskoy, E., et al. Master Robotic Net. *Advances in Astronomy* **2010**, 349171 (2010)
15. Piran, T. Gamma-ray bursts and the fireball model. *Physics Reports* **314**, 575-667 (1999)
16. Kumar, P., & Zhang, B. The physics of gamma-ray bursts relativistic jets. *Physics Reports* **561**, 1-109 (2015)
17. Kobayashi, S. Light Curves of Gamma-Ray Burst Optical Flashes. *Astrophys. J.* **545**, 807-812 (2000)

18. Sari, R., & Mészáros, P. Impulsive and Varying Injection in Gamma-Ray Burst Afterglows. *Astrophys. J.* **535**, L33-L37 (2000)

19. Zhang, B.-B., Zhang, B., Castro-Tirado, A. J., et al. Transition from Fireball to Poynting-flux-dominated Outflow in Three-Episode GRB 160625B. Preprint at https://arxiv.org/abs/1612.03089 (2016)

20. Gruzinov, A., & Waxman, E. Gamma-Ray Burst Afterglow: Polarization and Analytic Light Curves. *Astrophys. J.* **511**, 852-861 (1999)

21. Granot, J., & Königl, A. Linear Polarization in Gamma-Ray Bursts: The Case for an Ordered Magnetic Field. *Astrophys. J.* **594**, L83-L87 (2003)

22. Rybicki, G. B., & Lightman, A. P. Radiative Processes in Astrophysics. Wiley-Interscience, New York (1979)

23. Inoue, T., Asano, K., & Ioka, K. Three-dimensional Simulations of Magnetohydrodynamic Turbulence Behind Relativistic Shock Waves and Their Implications for Gamma-Ray Bursts. *Astrophys. J.* **734**, 77 (2011)

24. Lyutikov, M., Pariev, V. I., & Blandford, R. D. Polarization of Prompt Gamma-Ray Burst Emission: Evidence for Electromagnetically Dominated Outflow. *Astrophys. J.* **597**, 998-1009 (2003)

25. Zhang, B., & Yan, H. The Internal-collision-induced Magnetic Reconnection and Turbulence (ICMART) Model of Gamma-ray Bursts. *Astrophys. J.* **726**, 90 (2011)

26. Deng, W., Zhang, H., Zhang, B., & Li, H. Collision-induced Magnetic Reconnection and a Unified Interpretation of Polarization Properties of GRBs and Blazars. *Astrophys. J.* **821**, L12 (2016)

27. Bromberg, O., & Tchekhovskoy, A. Relativistic MHD simulations of core-collapse GRB jets: 3D instabilities and magnetic dissipation. *Mon. Not. R. Astron. Soc.* **456**, 1739-1760 (2016)

28. Sironi, L., & Spitkovsky, A. Particle Acceleration in Relativistic Magnetized Collision-less Electron-Ion Shocks. *Astrophys. J.* **726**, 75 (2011)

29. Giannios, D. UHECRs from magnetic reconnection in relativistic jets. *Mon. Not. R. Astron. Soc.* **408**, L46-L50 (2010)

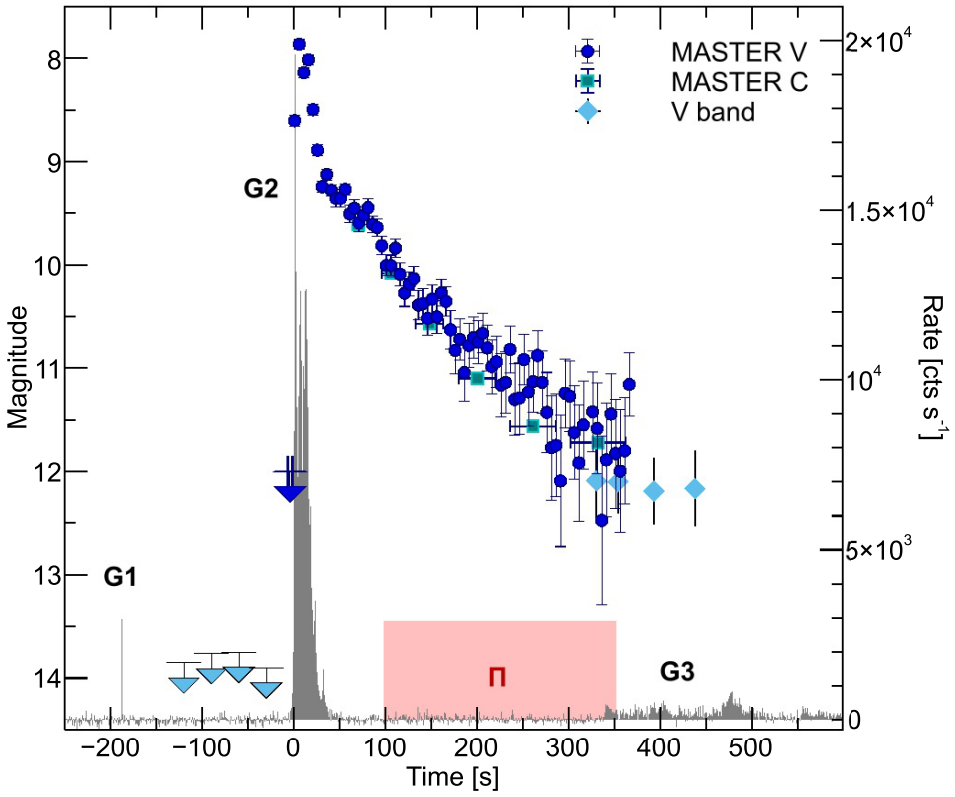

Figure 1: Prompt gamma-ray and optical light curves of GRB160625B.

The gamma-ray light curve (black; 10-250 keV) consists of three main episodes: a short precursor (G1), a bright main burst (G2), and a fainter and longer lasting tail of emission (G3). Optical data from the MASTER Net telescopes and other ground-based facilities[19] are overlaid for comparison. Error bars are 1 σ, upper limits are 3 σ. The red box marks the time interval over which polarimetric measurements were carried out. Within the sample of nearly 2,000 bursts detected by the GBM, only 6 other events have a comparable duration. The majority of GRBs ends before the start of polarimetric observations.

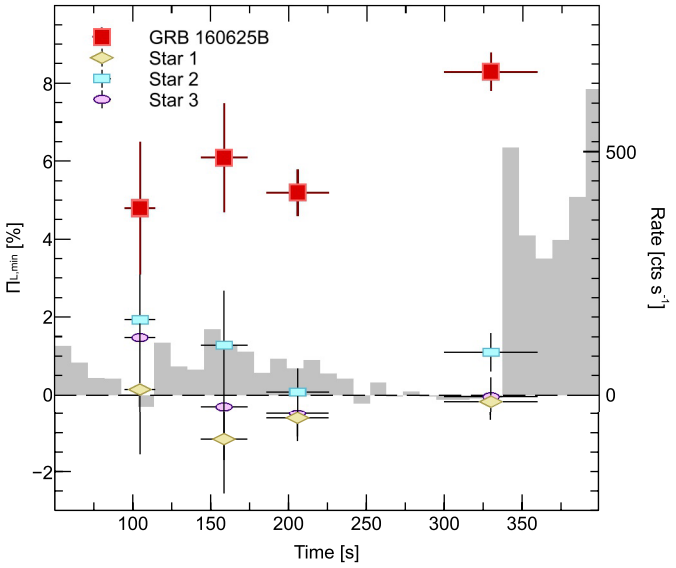

Figure 2: Temporal evolution of the optical polarization measured for GRB 160625B. The minimum polarization, measured in four different temporal bins (red squares), remains fairly constant over the first three exposures, then increases by 60% during the last observation. At the same time an evident increase in the gamma-ray count rates (gray shaded area; 5 s time bins) marks the onset of the third episode of prompt emission (G3). The spectral shape and fast temporal variability observed during G3 are typical of the GRB prompt emission. For comparison, we also report simultaneous polarimetric measurements of the three brightest stars in the MASTER-IAC field of view. Error bars are 1 σ.

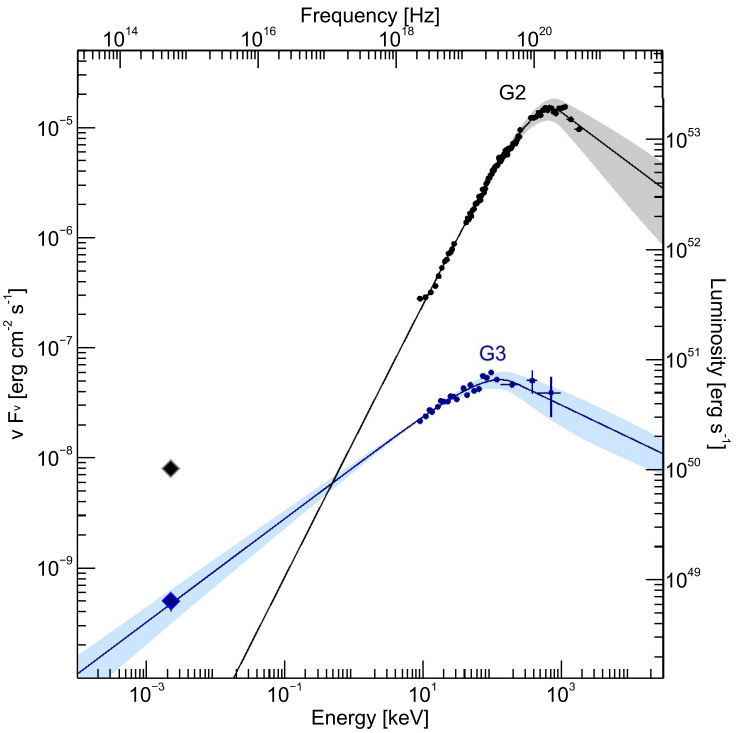

Figure 3: Broadband spectra of the prompt phase in GRB 160625B.

Spectra are shown for the two main episodes of prompt emission, labeled as G2 and G3. Error bars are 1 σ. The gamma-ray spectra were modeled with a smoothly broken power-law (solid line). The 1 σ uncertainty in the best fit model is shown by the shaded area. The diamonds indicate the average optical flux (corrected for Galactic extinction) observed during the same time intervals. The extrapolated contribution of the prompt gamma-ray component to the optical band is non negligible during G3 and constitutes >40% of the observed emission.

Methods

MASTER Observations

The MASTER-IAC telescope, located at Teide Observatory (Tenerife, Spain), responded to the first GBM alert and started observing the field with its very wide field camera at T_0-133 s. Observations were performed with a constant integration time of 5 s and ended at T_0+350 s. The MASTER II telescope responded to the LAT alert[13] and observed the GRB position between T_0+65 s and T_0+360 s. The resulting light curves are shown in Fig. 1. Polarimetric observations started at T_0+95 s in response to the LAT trigger. However, due to a software glitch, they were scheduled as a series of tiled exposures covering a larger area. This caused the telescope to slew away from the burst true position at T_0+360 s. A total of four useful exposures were collected (Extended Data Table 1). Data were reduced in a standard fashion[5,14]. The two synchronous frames used to measure the polarization were mutually calibrated so that the average polarization for comparison stars is zero. This procedure removes the effects of interstellar polarization. The significance of the polarimetric measurements was assessed through Monte Carlo simulations. Extended Data Figure 2 shows the resulting distribution of polarization values and significances.

Swift Observations

Swift observations span the period from T_0+9.6 ks to T_0+48 days. XRT data were collected in Photon Counting (PC) mode for a total net exposure of 134 ks. The optical afterglow was monitored with the UVOT in the *u*, *v*, and *w1* filters for 10 days after the burst, after which it fell below the UVOT detection threshold. Subsequent observations were performed using the UVOT filter of the day. *Swift* data were processed using the *Swift* software package within HEASOFT v6.19. We used the latest release of the XRT and UVOT Calibration Database and followed standard data reduction procedures. Aperture photometry on the UVOT images was performed

using a circular region of radius 2.5″ centered on the afterglow position. When necessary, adjacent exposures were co-added in order to increase the signal. We adopted the standard photometric zero points in the *Swift* UVOT calibration database[30]. The resulting *Swift* light curves are shown in Extended Data Figure 1.

RATIR Observations

RATIR obtained simultaneous multi-color (*riZYJH*) imaging of GRB160625B starting at T_0+8 hrs and monitored the afterglow for the following 50 days until it fell below its detection threshold. RATIR data were reduced and analyzed using standard astronomy algorithms. Aperture photometry was performed with SExtractor[31] and the resulting instrumental magnitudes were compared to Pan-STARRS1[32] in the optical and 2MASS[33] in the NIR to derive the image zero points. Our final optical and infrared photometry is shown in Extended Data Figure 1.

Radio observations

Radio observations were carried out with the Australian Telescope Compact Array (ATCA; PI: Troja) and the Jansky Very Large Array (VLA; PI: Cenko). The ATCA radio observations were carried out on June 30th 2016 (T_0+4.5d) at the center frequencies of 5.5, 7.5, 38 and 40 GHz, on July 11th 2016 (T_0+15.7d) at the center frequencies of 18, 20, 38 and 40 GHz and on July 24th 2016 (T_0+28.6 d) at the center frequencies of 8, 10, 18 and 20 GHz. For all epochs the frequency bandwidth was 2 GHz and the array configuration was H75. The standard calibrator PKS 1934-638 was observed to obtain the absolute flux density scale. The phase calibrators were PKS 2022+031 for 5.5-10 GHz observations and PKS 2059+034 for 18-40 GHz observations. The data were flagged, calibrated and imaged with standard procedures in the data reduction package MIRIAD[34]. Multi Frequency Synthesis images were formed at 6.5, 7.5, 9, 19 and 39 GHz. The target appeared point-like in all restored images.

The VLA observed the afterglow at three different epochs: 2016 June 30, July 09, and July 27. In all of our observations we used J2049+1003 as the phase calibrator and 3C48 and the flux calibrator. The observations were undertaken at a central frequency of 6 GHz (C-band) and 22 GHz (K-band) with a bandwidth of 4 GHz and 8 GHz, respectively. The data was calibrated using standard tools in the CASA software and then imaged with the clean task. The source was significantly detected in all three observations and in all bands. The radio afterglow light curve at 10 GHz is shown in Extended Data Figure 1.

Spectral properties of the prompt GRB phase

GRB 160625B is characterized by three distinct episodes of prompt gamma-ray emission, separated by long periods of apparent quiescence (Fig. 1). A detailed spectral analysis of the first two episodes (G1 and G2) is presented elsewhere[19], and shows that the first event G1 is well described by a thermal component with temperature kT $\approx$15 keV, while the second burst G2 is dominated by a non-thermal component peaking at energies $E_p \gtrsim 500$ keV and consistent with synchrotron emission in a decaying magnetic field[35]. Our spectral analysis focuses instead on the third event (G3).

The time intervals for our analysis were selected based on the properties of the gamma-ray and optical light curves. GBM data were retrieved from the public archive and inspected using the standard RMFIT tool. The variable gamma-ray background in each energy channel was modeled by a series of polynomial functions. Spectra were binned in order to have at least 1 count per spectral bin and fit within XSPEC[36] by minimizing the modified Cash statistics. We used a Band function[37] to model the spectra, and fixed the high-energy index to β=-2.3 when the data could not constrain it. The best fit model was then extrapolated to lower energies in order to estimate the contribution of the prompt component at optical frequencies. During the main gamma-ray

episode (G2), the observed optical emission is several orders of magnitude brighter than the extrapolation of the prompt component. In contrast, we found that the later prompt phase (G3) significantly contributes to the observed optical flux. This is rare but not unprecedented[38-40]: it has been shown that the majority of GRBs have an optical emission fainter than R = 15.5 mag when the gamma- ray emission is active, however a small fraction (≈5-20%) exhibit a bright (R≥14 mag) optical counterpart during the prompt phase[41].

As a further test we performed a joint time-resolved analysis of the optical and gamma-ray data during G3. The results are summarized in Extended Data Table 2. The derived broadband spectra are characterized by a low-energy photon index of –1.5, consistent with fast cooling ($\nu_c<\nu_m$) synchrotron radiation. Our analysis constrains the spectral peak at $\nu_m\approx2\times10^{19}$ Hz and, for typical conditions of internal dissipation models, the cooling frequency of the emitting electrons is $\nu_c \approx 5 \times 10^{12}\ (\varepsilon_B/0.1)^{-3/2}$ Hz << ν_{opt} << ν_m, where we adopted the standard assumption that the magnetic energy is a constant fraction ε_B of the internal energy generated in the prompt dissipation process. Since the synchrotron self-absorption might suppress the emission at low frequencies, we consider below whether it affects the optical band. A simple estimate of the maximal flux is given by a blackbody emission with the electron temperature $k_B T \approx \gamma_e m_e c^2$,

$$F_{\nu,BB} = 2\pi\nu^2 (1+z)^3 \Gamma\gamma_e m_e \left(\frac{R_\perp}{D_L}\right)^2, \quad (1)$$

where $\nu \sim 5.5 \times10^{14}$ Hz is the observed frequency, z=1.406 the GRB redshift, $\gamma_e \propto \nu^{1/2}$ the electron's Lorentz factor, Γ the bulk Lorentz factor, $D_L\approx3\times10^{28}$ cm the luminosity distance and $R_\perp$ the fireball size for the observer, which depends on the emission radius R_e as $R_\perp \sim R_e/\Gamma$. By imposing that the blackbody limit is larger than the observed optical flux $F_\nu \sim 90$ mJy, we obtain a lower limit to the emission radius[39]:

$$R_{\min} \approx 4\times10^{14}\left(\frac{\Gamma}{200}\right)^{2/5}\left(\frac{\varepsilon_B}{0.1}\right)^{1/10}\left(\frac{E_{\gamma,iso}}{10^{53}\,erg}\right)^{1/10}\left(\frac{\Delta T}{300\,s}\right)^{-1/10}\text{cm}, \quad (2)$$

where ΔT is the duration of the G3 burst, and $E_{\gamma,iso}$ is the isotropic equivalent gamma-ray energy released over ΔT. The radius derived in Eq. 2 is within the acceptable range for internal dissipation models, in particular those invoking the dissipation of large-scale magnetic fields[25, 29] as suggested by our polarization measurements. For emission radii larger than R_{min} the synchrotron self-absorption does not affect the optical emission, in agreement with our observations of a single power-law segment from optical to hard X-rays. These results lend further support to our conclusions.

Origin of the Early Optical Emission

One of the main features of GRB 160625B is its extremely bright optical emission during the prompt phase (Fig. 1). In the previous section we showed that, during G3, the data support a common origin for the optical and gamma-ray photons, consistent with a standard fast cooling synchrotron emission. Our analysis also showed that the same conclusion does not hold at earlier times. During the main burst (G2) the observed emission cannot be explained by a single spectral component (Fig. 3). A distinct physical origin for the optical and gamma-ray emissions is also suggested by the time lag between their light curves (Extended Data Figure 3).

A plausible interpretation is that the bright optical flash is powered by the reverse shock, and is unrelated to the prompt gamma-ray emission during G2. In this framework our first three polarization measurements probe the fireball ejecta at the larger reverse shock radius, and only the fourth observation includes the significant contribution of the prompt phase. This model can consistently explain the early optical and radio observations, as shown in more detail in the following sections. However, in its basic form[17], the reverse shock emission cannot explain the rapid rise and double-peaked structure of the optical light curve.

A different possibility is that the early optical emission is produced by the same (or similar) mechanisms powering the prompt gamma-ray phase, which would naturally explain the initial sharp increase of the observed flux as well as its variability. One of the most popular hypotheses is that the optical and gamma-ray photons are produced by two different radiation mechanisms[42]: synchrotron for the optical and synchrotron self-Compton (SSC) for the gamma-rays. This model faces several problems, in particular the lack of temporal correlation between the low- and high-energy light curves, and the absence of a bright second order IC component. Another possibility is a two-components synchrotron radiation from internal shocks in a highly variable outflow[43]. This model predicts a weak high-energy emission and a delayed onset in the optical, consistent with the observations. However, it presents other limitations, such as an excessive energy budget and an unusually high variability of Lorentz factors.

In a different set of models the optical and gamma-ray photons come from two distinct emitting zones within the flow. In the magnetic reconnection model[44] a bright quasi-thermal component, emitted at the photospheric radius, peaks in the hard X-rays, while standard synchrotron emission from larger radii is observed in the optical. This can explain most of the properties of G2, but it does not reproduce well the observed spectral shape: the low-energy spectral slope measured during this interval[19] is too shallow to be accounted for by the Rayleigh-Jeans tail of the thermal spectrum.

The properties of G2 are best explained by models in which the optical and gamma-ray photons arise from synchrotron radiation at different lab times[45] or in different emitting regions. These are for example late internal shocks from residual collisions[46] or free neutron decay[47]. In this framework the steep decay phase observed after the second optical peak could be powered by delayed prompt emission from higher latitudes with respect to the observer's line of sight. This

399 case, in which all the polarization measurements probe the prompt emission mechanisms, only
400 strengthens our finding that the prompt optical emission is inherently polarized.

401 **Polarization**

402 Synchrotron radiation is inherently highly polarized. For a power-law energy distribution of the
403 emitting electrons $\left(dn/dE \propto E^{-p}\right)$, the intrinsic linear polarization at low frequencies is
404 Π_{syn}=9/13~70%. If an ordered magnetic field permeates the GRB jet each emitting region
405 generates the maximum polarization Π_{syn}. However, due to relativistic kinematic effects, the
406 average polarization within the Γ^{-1} field of view is smaller and here we assume $\Pi_{MAX}\approx 50\%$ for
407 the regime $\nu_c < \nu < \nu_m$.

408 Since an observer can only see a small area around the line of sight due to the relativistic
409 beaming, the magnetic field can be considered parallel within the visible area. Our measured
410 value $\Pi_{L,min}$ is related to the true degree of polarization as $\Pi_{L,min} = \Pi_L \cos 2\theta$ where θ is the angle
411 between the polarization direction and the x-axis of the reference system. For a random
412 orientation of the observer, if $\Pi_L \approx \Pi_{MAX}$ the chance to detect a polarization lower than $\Pi_{L,min}$~8%
413 is small (~10%). The observed values of $\Pi_{L,min}$ suggest that the magnetic field is largely distorted
414 even on small angular scales ~$1/\Gamma$, but not completely tangled yet.

415 As the detected optical light is a mixture of reverse shock and prompt emission, we now consider
416 whether our polarization measurements require the magnetic field to be distorted in both the
417 emitting regions. In our last polarimetric observation the prompt and reverse shock components
418 contribute roughly equally to the observed light so that $\Pi_{L,min} = (\Pi_{L,r}\cos 2\theta_r + \Pi_{L,p}\cos 2\theta_p)/2 \sim$
419 8% where the subscripts refer to the prompt (p) and reverse shock (r) contributions. The first
420 three observations are dominated by the reverse shock component and show a low but stable

degree of polarization, $\Pi_{L,r}\cos 2\theta_r \approx 5\%$. By assuming that the reverse shock polarization remains constant during our last polarimetric exposure, as expected in the presence of a large-scale magnetic field[3], we derive $\Pi_{L,p}\cos 2\theta_p \approx 11\%$, well below the maximum possible value. Since in general $\theta_r \neq \theta_p$ the chance that our measurement is due to the instrumental set-up is $\leq 1\%$. Our data therefore suggest that the distortion of the magnetic field configuration happens in the early stages of the jet, at a radius comparable or smaller than the prompt emission radius.

Broadband afterglow modeling

Unless otherwise stated, all the quoted errors are 1 σ. The temporal evolution of the X-ray, optical and nIR afterglow is well described by simple power- law decays ($F \propto t^{-\alpha}$) with slopes $\alpha_X = 1.22 \pm 0.06$, $\alpha_{opt} = 0.945 \pm 0.005$ and $\alpha_{IR} = 0.866 \pm 0.008$ until T_0+14 d, when the flux is observed to rapidly decrease at all wavelengths with a temporal index $\alpha_j = 2.57 \pm 0.04$.

The X-ray spectrum is best fit by an absorbed power-law model with slope $\beta_X = 0.92 \pm 0.06$ and only marginal (2 σ) evidence for intrinsic absorption, $N_{H,i} = (1.6 \pm 0.8) \times 10^{21}$ cm^{-2}, in addition to the galactic value $N_H = 9.6 \times 10^{20}$ cm^{-2}. A power-law fit performed on the optical/nIR data yields negligible intrinsic extinction and a slope $\beta_{OIR} = 0.50 \pm 0.05$ at T_0+8 hrs, which progressively softens to 0.8±0.2 at T_0+10 d. The low intrinsic extinction ($E_{B-V} < 0.06$, 95% confidence level) shows that dust scattering has a negligible effect[48] (<0.5%) on our measurements of polarization.

Within the external shock model, the difference in temporal and spectral indices indicates that the X-ray and optical/IR emissions belong to two different synchrotron segments. A comparison with the standard closure relations shows that the observed values are consistent with the regime $\nu_m < \nu_{opt} < \nu_c < \nu_X$ for $p \approx 2.2$. The color change of the optical/IR afterglow suggests that the cooling break decreases and progressively approaches the optical range. This feature is distinctive of a forward shock expanding into a medium with a homogeneous density profile[49].

444 However, the measured radio flux and spectral slope cannot be explained by the same
445 mechanism, and require an additional component of emission, likely originated by a strong
446 reverse shock re-heating the fireball ejecta as it propagates backward through the jet. This is also
447 consistent with our observations of a bright optical flash at early times[17]. In order to test this
448 hypothesis, we created seven different spectral energy distributions (SEDs) at different times,
449 ranging from T_0+0.4 d to T_0+30 d, and modeled the broadband afterglow and its temporal
450 evolution with a forward shock + reverse shock (FS + RS) model[17,49]. The best fit afterglow
451 parameters are an isotropic-equivalent kinetic energy $log\ E_{K,iso} = 54.3^{+0.17}_{-0.5}$, a low circumburst
452 density $log\ n = -4.0^{+1.7}_{-1.1}$, and microphysical parameters $log\ \varepsilon_e = -1.0^{+0.5}_{-1.0}$ and $log\ \varepsilon_B = -2.0 \pm 1.0$.
453 These results are consistent with the trend of a low density environment, and high radiative
454 efficiency observed in other bright bursts[50,51]. Our data and best fit model are shown in Extended
455 Data Figure 4.
456 In this framework, the achromatic temporal break at T_0+14 d is the result of the outflow
457 geometry, collimated into a conical jet with a narrow opening angle $\theta_j = 2.4^{+1.6}_{-0.7}$ deg, This
458 lessens the energy budget by a factor θ_j^2 and the resulting collimation corrected energy release
459 ~6×10^{51} erg is within the range of other GRBs. The extreme luminosity of GRB160625B can be
460 therefore explained, at least in part, by its outflow geometry as we are viewing the GRB down
461 the core of a very narrow jet.
462 The large flux ratio between the RS and FS at peak, $f_{RS}/f_{FS} > 5\times10^3$, implies a high magnetization
463 parameter[52,53] $R_B \approx \varepsilon_{B,RS}/\varepsilon_{B,FS} > 100\ (\Gamma/500)^2 >> 1$, and shows that the magnetic energy density
464 within the fireball is larger than in the forward shock. From our broadband modeling we derived
465 a best fit value of $\varepsilon_{B,FS} \approx 0.01$ with a 1 dex uncertainty, which allows us to estimate the ejecta

magnetic content in the range $\sigma \geq 0.1$, where solutions with $\sigma > 1$ would suppress the reverse shock emission and are therefore disfavored.

Additional References

30. Breeveld, A. A., Landsman, W., Holland, S. T., et al. An Updated Ultraviolet Calibration for the *Swift*/UVOT, *American Institute of Physics Conference Series* **1358**, 373-376 (2011)
31. Bertin, E., & Arnouts, S. SExtractor: Software for source extraction. *Astron. Astrophys. Supp.* **117**, 393-404 (1996)
32. Chambers, K. C., Magnier, E. A., Metcalfe, N., et al. The Pan-STARRS1 Surveys. Preprint available at https://arxiv.org/abs/1612.05560 (2016)
33. Skrutskie, M. F., Cutri, R. M., Stiening, R., et al. The Two Micron All Sky Survey (2MASS). *Astron. J.* **131**, 1163-1183 (2006)
34. Sault, R. J., Teuben, P. J., & Wright, M. C. H. A Retrospective View of MIRIAD. *Astronomical Data Analysis Software and Systems IV* **77**, 433-436 (1995)
35. Uhm, Z. L., & Zhang, B. Fast-cooling synchrotron radiation in a decaying magnetic field and γ-ray burst emission mechanism. *Nature Physics* **10**, 351-356 (2014)
36. Arnaud, K. A. XSPEC: The First Ten Years. *Astronomical Data Analysis Software and Systems V* **101**, 17-20 (1996)
37. Band, D., Matteson, J., Ford, L., et al. BATSE observations of gamma-ray burst spectra. I - Spectral diversity. *Astrophys. J.* **413**, 281-292 (1993)
38. Vestrand, W. T., Wozniak, P. R., Wren, J. A., et al. A link between prompt optical and prompt γ-ray emission in γ-ray bursts. *Nature* **435**, 178-180 (2005)

39. Shen, R.-F., & Zhang, B. Prompt optical emission and synchrotron self-absorption constraints on emission site of GRBs. *Mon. Not. R. Astron. Soc.* **398**, 1936-1950 (2009)

40. Gendre, B., Atteia, J. L., Boër, M., et al. GRB 110205A: Anatomy of a Long Gamma- Ray Burst. *Astrophys. J.* **748**, 59 (2012)

41. Klotz, A., Boër, M., Atteia, J. L., & Gendre, B. Early Optical Observations of Gamma-Ray Bursts by the TAROT Telescopes: Period 2001-2008. *Astron. J.* **137**, 4100-4108 (2009)

42. Kumar, P., & Panaitescu, A. What did we learn from gamma-ray burst 080319B? *Mon. Not. R. Astron. Soc.* **391**, L19-L23 (2008)

43. Yu, Y. W., Wang, X. Y., & Dai, Z. G. Optical and γ-ray Emissions from Internal Forward-Reverse Shocks: Application to GRB 080319B? *Astrophys. J.* **692**, 1662-1668 (2009)

44. Giannios, D. Prompt GRB emission from gradual energy dissipation. *Astron. Astrophys.* **480**, 305-312 (2008)

45. Wei, D. M. The GRB early optical flashes from internal shocks: application to GRB990123, GRB041219a and GRB060111b. *Mon. Not. R. Astron. Soc.* **374**, 525-529 (2007)

46. Li, Z., & Waxman, E. Prompt Optical Emission from Residual Collisions in Gamma- Ray Burst Outflows. *Astrophys. J.* **674**, L65-L68 (2008)

47. Fan, Y. Z., Zhang, B., & Wei, D. M. Early Optical-Infrared Emission from GRB 041219a: Neutron-rich Internal Shocks and a Mildly Magnetized External Reverse Shock. *Astrophys. J.* **628**, L25-L28 (2005)

48. Serkowski, K., Matheson, D. S. & Ford, V. L. Wavelength dependence of interstellar polarisation and ratio of total to selective extinction. *Astrophys. J.* **196**, 261 (1975)

49. Granot, J., & Sari, R. The Shape of Spectral Breaks in Gamma-Ray Burst Afterglows. *Astrophys. J.* **568**, 820-829 (2002)

50. Cenko, S. B., Frail, D. A., Harrison, F. A., et al. Afterglow Observations of Fermi Large Area Telescope Gamma-ray Bursts and the Emerging Class of Hyper-energetic Events. *Astrophys. J.* **732**, 29 (2011)
51. Ackermann, M., Ajello, M., Asano, K., et al. Multiwavelength Observations of GRB 110731A: GeV Emission from Onset to Afterglow. *Astrophys. J.* **763**, 71 (2013)
52. Zhang, B., Kobayashi, S., & Mészáros, P. Gamma-Ray Burst Early Optical Afterglows: Implications for the Initial Lorentz Factor and the Central Engine. *Astrophys. J.* **595**, 950-954 (2003)
53. Zhang, B., & Kobayashi, S. Gamma-Ray Burst Early Afterglows: Reverse Shock Emission from an Arbitrarily Magnetized Ejecta. *Astrophys. J.* **628**, 315-334 (2005)

Data availability: All relevant data are available from the corresponding author upon reasonable request. Data presented in Figure 1, and Extended Data Figure 1 are included with the manuscript. *Swift* XRT data are available at http://www.swift.ac.uk/xrt_products/

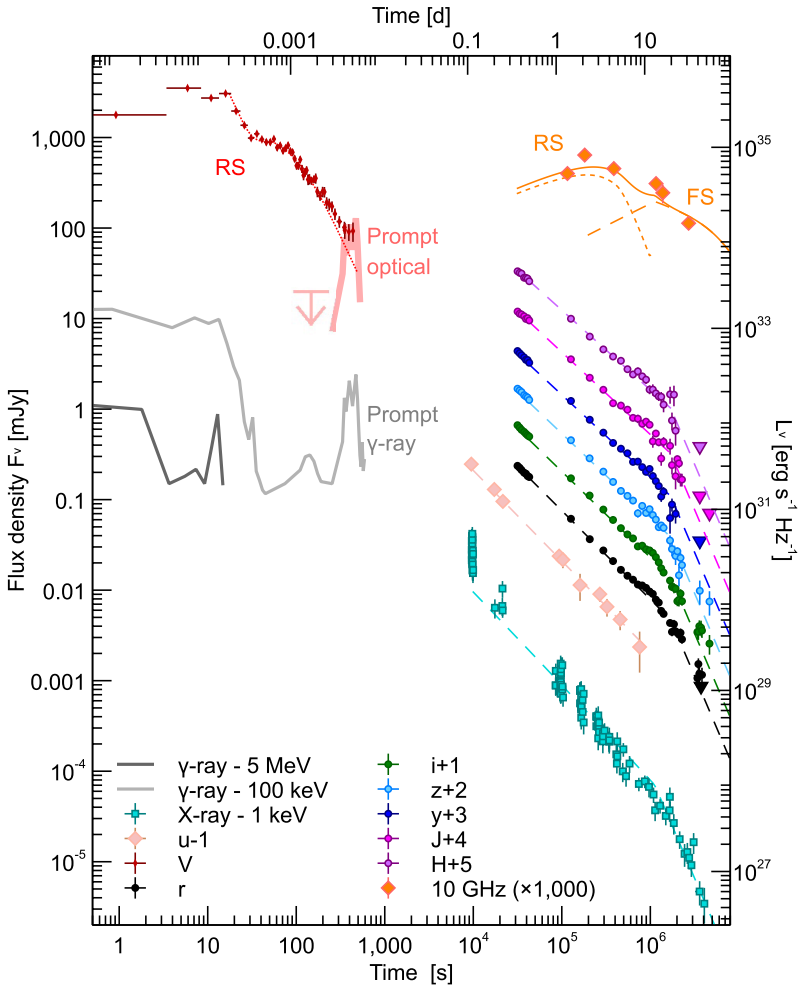

Extended Data Figure 1: Multi-wavelength light curves of GRB160625B and its afterglow. Different emission components shape the temporal evolution of GRB160625B. On timescales of seconds to minutes after the explosion, we observe bright prompt (solid lines) and reverse shock (dotted lines) components. On timescales of hours to weeks after the burst, emission from the forward shock (dashed lines) becomes the dominant component from X-rays down to radio energies. After ≈14 d, the afterglow emission rapidly falls off at all wavelengths. This phenomenon, known as jet-break, is caused by the beamed geometry of the outflow. Error bars are 1 σ, and upper limits are 3 σ. Times are referred to the LAT trigger time T_0.

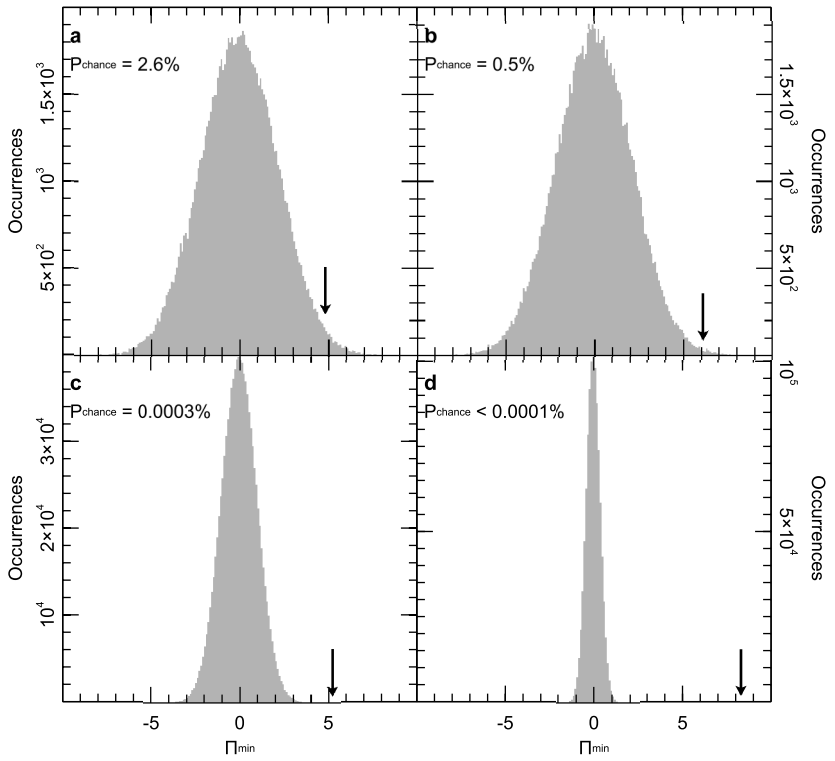

Extended Data Figure 2: Results of the Monte Carlo simulations.

For each of the four polarization epochs we simulated and examined a large number of datasets with similar photometric properties and no intrinsic afterglow polarization. **a** Results of 10^5 simulations for the first epoch (95 s – 115 s) **b** Same as **a** but for the second epoch (144 s - 174 s) **c** Results of 10^6 simulations for the third epoch (186 s - 226 s) **d** Same as **c** but for the fourth epoch (300 s - 360 s). The observed value is shown by a vertical arrow. The probability of obtaining by chance a polarization measurement as high as the observed value is also reported.

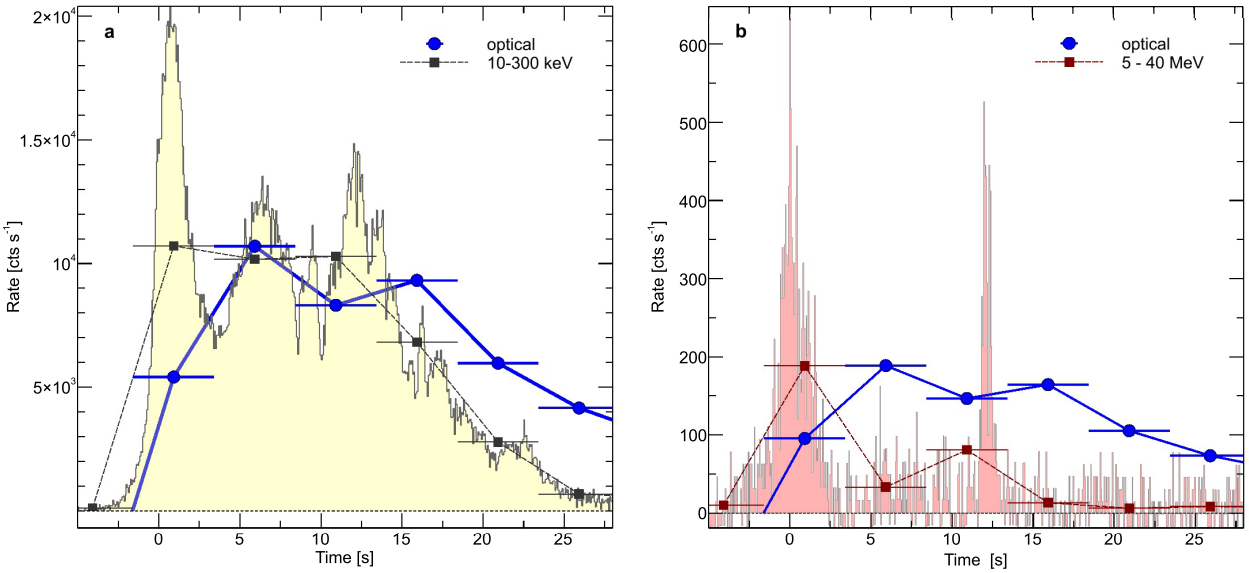

Extended Data Figure 3: A comparison of the early gamma-ray and optical emission measured for GRB 160625B

a Gamma-ray light curves in the soft (50–300 keV) energy band. **b** Gamma-ray light curves in the hard (5–40 MeV) energy band. Optical data (blue circles) are arbitrarily rescaled. The squared points show the gamma-ray light curves rebinned by adopting the same time intervals of the optical observations. Times are referred to the LAT trigger time T_0.

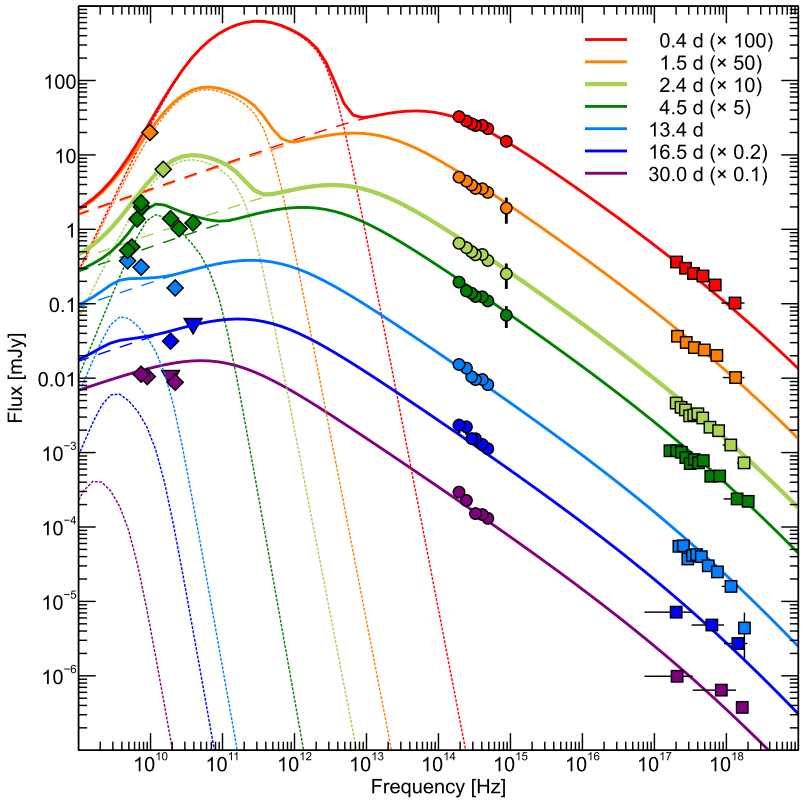

Extended Data Figure 4: Afterglow spectral energy distributions of GRB 160625B.

The afterglow evolution can be described by the combination of forward shock (dashed lines) and reverse shock (dotted lines) emission. The best fit model is shown by the solid lines. The peak flux of the forward shock component is ≈0.4 mJy, significantly lower than the optical flux measured at $T < T_0$+350 s. This shows that the forward shock emission is negligible during the prompt phase. Error bars are 1 σ, and upper limits are 3 σ.

Extended Data Table 1: Polarimetry Results.

Time since T_0 [mid; s]	Exposure time [s]	$\Pi_{L,min}$ [%]	Error [1 σ; %]
105	20	4.8	1.7
159	30	6.1	1.4
206	40	5.2	0.6
330	60	8.3	0.5

Extended Data Table 2: Spectral properties of the prompt emission for GRB 160625B.

Time interval [s]	Detectors	α	β	E_p [keV]	Flux (10-10^4 keV) [10^{-7} erg cm^{-2} s^{-1}]	W-Stat	dof
0.10-19.10 (G2)	NaI_7, NaI_9, BGO_1	-0.733±0.010	-2.50±0.04	680±20	429±5	250	204
337-607 (G3)	NaI_6, BGO_1	-1.52±0.04	2.3	140^{+40}_{-30}	2.30±0.10	211	77
Time-Resolved Analysis							
334-359	NaI_6, BGO_1	-1.53±0.02	2.3	>210	3.2±0.5	60	74
359-384	NaI_6, BGO_1	-1.55±0.03	2.3	>180	2.4±0.7	58	74
384-414	NaI_6, BGO_1	-1.49±0.02	2.3	>210	3.9±0.7	67	72
414-464	NaI_6, BGO_1	-1.53±0.04	2.3	270±80	3.2±0.3	68	73
464-499	NaI_6, BGO_1	-1.45±0.03	2.3	130±15	4.9±0.3	62	81

The GRB prompt emission can be described by a smoothly broken power-law[37] with low-energy index α, high-energy index β, and peak energy E_p. Errors are 1 σ, lower limits are at 95% confidence level. Given the high statistical quality of the G2 spectrum a 5% systematic error was added to the fit.

Acknowledgements ET thank L. Piro and K. Murase for comments. We thank the RATIR project team and the staff of the Observatorio Astronmico Nacional on Sierra San Pedro Mártir, and acknowledge the contribution of Leonid Georgiev and Joshua S. Bloom to its development. RATIR is a collaboration between the University of California, the Universidad Nacional Autonóma de México, NASA Goddard Space Flight Center, and Arizona State University, benefiting from the loan of an H2RG detector and hardware and software support from Teledyne Scientific and Imaging. RATIR, the automation of the Harold L. Johnson Telescope of the Observatorio Astronómico Nacional on Sierra San Pedro Mártir, and the operation of both are funded through NASA grants NNX09AH71G, NNX09AT02G, NNX10AI27G, and NNX12AE66G, CONACyT grants INFR-2009-01-122785 and CB-2008-101958, UNAM PAPIIT grant IN113810, and UC MEXUS-CONACyT grant CN 09-283. The MASTER project is supported in part by the Development Program of Lomonosov Moscow State University, Moscow Union OPTICA, Russian Science Foundation 16-12-00085. This work was supported in part by NASA Fermi grants NNH15ZDA001N and NNH16ZDA001N. This work made use of data supplied by the UK Swift Science Data Centre at the University of Leicester, funded by the UK Space Agency.

Author Contributions ET, CGM, and SK composed the text based on inputs from all the co-authors. MASTER data were provided, reduced and analyzed by VML, ESG and NVT. RATIR observations were obtained, reduced and analyzed by NRB, ET, AMW, AK, WHL, and VT. FEM processed and analyzed the *Swift*/UVOT data. ET, RR and MW obtained, processed and analyzed the ATCA observations. VLA observations were obtained, processed and analyzed by

SBC, AF, AH. All authors assisted in obtaining parts of the presented dataset, discussed the results or commented on the manuscript.

Competing financial interests The authors declare no competing financial interests.

Correspondence Correspondence and requests for materials should be addressed to E. Troja (eleonora.troja@nasa.gov).